Energy & Environmental Science

COMMUNICATION

View Article Online
View Journal | View Issue

Cite this: *Energy Environ. Sci.*, 2018, **11**, 2010

Received 6th March 2018,
Accepted 7th June 2018

DOI: 10.1039/c8ee00686e

rsc.li/ees

An all-aqueous redox flow battery with unprecedented energy density†

Jing Zhang, Gaopeng Jiang, Pan Xu, Ali Ghorbani Kashkooli, Mahboubeh Mousavi, Aiping Yu and Zhongwei Chen *

Redox flow batteries are of particular interest because of the flexible power and energy storage originating from their unique architecture, but their low energy density has inhibited their widespread dissemination. In this work, a novel strategy of tuning the pH of the electrolyte environment is put forward to enhance the battery voltage, and eventually achieve the goal of high energy density for all-aqueous redox flow batteries. With this strategy, a hybrid alkaline zinc–iodine redox flow battery has been designed with a 0.47 V potential enhancement by switching the anolyte from acidic to basic, thus inspiring an experimental high energy density of 330.5 W h L^{-1}. This is an unprecedented record to date for an all-aqueous redox flow battery.

Broader context

Redox flow batteries as an advanced power and energy storage system are being driven by an ever-increasing demand to mitigate output fluctuations and stabilize power grids. In contrast to capsule-enclosed batteries, redox flow batteries have unique architectures that can store electrolyte with redox-active materials in external reservoirs, thus leading to a controllable energy capacity up to the megawatt-hour (MW h) range by expanding the reservoir volume. With a certain electrolyte volume and concentration, the energy density of a redox flow battery is usually determined by the electron transfer number of the redox reaction or the flow battery voltage. Therefore, enhancing the battery voltage could be one very feasible and effective approach for achieving high energy capacity. Theoretically, the electrolyte acidic/basic properties have a great influence on redox pair potential. By tuning the pH of the electrolyte, the battery voltage can be effectively enhanced, finally leading to an increase in energy density. Inspired by this concept, an all-aqueous hybrid alkaline zinc/iodine flow battery is designed and demonstrated in this work with an unprecedented high-energy-density of 330.5 W h L^{-1} as well as a 0.47 V battery potential enhancement compared to the conventional counterparts.

In order to meet the soaring worldwide energy demand, various renewable energy resources are integrated into today's electrical grids, such as wind power and solar energy. However, these renewable power outputs are usually unstable and inconsistent due to their fluctuations along with the change of weather or location.[1–4] Thus, a great need for advanced energy storage systems to mitigate undulating outputs and stabilize power grids is looming. Redox flow batteries (RFBs) are of particular interest because of the flexible power and energy storage originating from their unique architecture.[5–8] In contrast to capsule-enclosed batteries, RFBs store electrolyte with redox-active materials in external reservoirs.[9–11] Redox reactions occur instantly on the electrodes' active surfaces when liquid electrolyte is flowing into the cell. Therefore, the battery capacity can be increased up to the megawatt-hour (MW h) range by simply expanding the volume of the reservoir.[12,13]

Among various RFB systems, all-vanadium redox flow batteries are recognized as one of the most promising commercialized candidates benefitting from their long cycle life, high efficiency and excellent electrochemical reversibility. However, with the soaring high energy demand, their merits are largely limited by the low energy density. With a certain electrolyte volume and concentration, the energy density of a RFB is usually determined by two factors: (1) the number of transferred electrons of the redox reaction;[14] (2) the flow battery voltage.[15] Thus, enhancing the battery voltage could be one very feasible and effective approach to achieving high energy density. Inspired by this concept, various non-aqueous RFBs have been put forward with elevated battery voltages because of their wide electrochemical window employing organic solvents.[16–23] Non-aqueous lithium-RFBs are typical examples with an elevated battery voltage (>2.0 V), which subtly combine lithium-ion or lithium–sulfur batteries with flow battery technology.[17,20,22] However, these non-aqueous lithium-RFBs have inevitable drawbacks: firstly, because of the use of lithium metal, they are very sensitive to moisture and gases such as O_2, N_2 and CO_2 in the air.[16,18] Secondly, ionic mobility in non-aqueous solutions is much slower than in their aqueous counterparts.[6] Lastly, most of the non-aqueous lithium-RFBs are based on the size of a coin-cell with a volume of electrolyte less than 5 mL, and

Department of Chemical Engineering, Waterloo Institute for Nanotechnology, Waterloo Institute for Sustainable Energy, University of Waterloo, Waterloo, Ontario N2L 3G1, Canada. E-mail: zhwchen@uwaterloo.ca

† Electronic supplementary information (ESI) available. See DOI: 10.1039/c8ee00686e

cannot be scaled-up. Alternatively, semi-aqueous lithium-RFBs have been proposed by using a completely ionized aqueous redox-active species in the aqueous catholyte to match up with a non-aqueous lithium anode.[26,27] They exhibit high energy densities and long cycle lives, benefitting from the unique battery structure which possesses the advantages of both aqueous and non-aqueous RFBs. However, owing to this specific battery configuration, a fragile and costly crack-free glass ceramic membrane must be assembled to eliminate organic/aqueous electrolyte cross-over issues, the manufacture of which will largely limits the scalability and increases the cost of flow batteries.[24,27] Also, the resistance of the ceramic membrane is usually high, thus meaning that the semi-aqueous RFBs cannot discharge at a very high current density. Therefore, non-aqueous and semi-aqueous RFBs are far from commercialization, while all-aqueous RFBs are still irreplaceable.[28] By introducing the concept of a middle electrolyte, a multiple ion-exchange membrane design for all-aqueous RFBs has been put forward, which creates the flexibility to allow new electrolyte combinations and gives a promising potential of high energy density for an all-aqueous RFB system.[29] However, this complex battery structure also brings new challenges to commercial scalability including more changes of electrolyte leakage and membrane fabrication.

The pursuit of high energy densities for all-aqueous RFBs was stuck in a bottleneck period until early in 2015, when Li *et al.* reported a promising high energy density (167 W h L^{-1}) zinc–polyiodide all-aqueous flow battery, which is approaching the energy density of low end lithium-ion batteries, successfully demonstrating a bright future for all-aqueous high energy density RFB systems.[30] Further improvement of the all-aqueous RFB performance is still burgeoning at present. But, little effort has been expended on the methodology of enhancing the battery voltage to improve the energy capacity of all-aqueous RFBs. This is because in theory, a high battery voltage is not attainable in aqueous electrolytes owing to the narrow water electrolysis potential window of 1.23 V.[27] However, considering kinetics, the practical water splitting potential is usually above 2 V because of the high over-potential of the hydrogen/oxygen evolution reaction at electrode surfaces.[31] If the low hydrogen evolution potential in alkaline medium could be combined with the high oxygen evolution potential in acid medium in one system, the battery could achieve a stable cell potential window even as high as ~3 V.[15] Thus, the water electrolysis reaction is not the restraining factor in aqueous solution if the battery can be designed and fabricated properly. Then, the next logical question is how to enhance the voltage of all-aqueous RFBs. According to the Pourbaix diagram, the pH value of an aqueous electrolyte has a great influence on the redox potential of electrode candidates.[32,33] By carefully observing the redox potential table, we can find that some redox potentials of metal pairs exhibit a huge difference between acid and alkaline environments. For example, a zinc redox potential of −0.763 V (Zn^{2+}/Zn) *versus* a standard hydrogen electrode (SHE) was obtained in acid electrolyte (eqn (1)),[30] whereas a redox potential of −1.260 V ($Zn(OH)_4^{2-}$/Zn) *versus* SHE was obtained in alkaline solution (eqn (2)).[34]

$$\text{In acid: } Zn^{2+} + 2e^- \rightarrow Zn \quad E^0 = -0.763\ \text{V} \tag{1}$$

$$\text{In alkaline: } Zn(OH)_4^{2-} + 2e^- \rightarrow Zn + 4OH^- \quad E^0 = -1.260\ \text{V} \tag{2}$$

Therefore, by simply tuning the acid–base environment for this redox pair, the battery voltage will significantly increase (*e.g.* 0.497 V potential enhancement for the zinc redox pair from acid and to alkaline electrolyte), which ultimately leads to an enhanced energy density. For the first time, this ingenious design of tuning the electrolytic pH value for achieving a high energy density for all-aqueous RFBs is proposed in this work. Simply and effectively, this novel strategy opens a promising route for the development of all-aqueous high-energy-density RFBs.

In this study, on the basis of the above consideration, a triiodide/iodide (I_3^-/I^-) redox pair is chosen as the cathode reactive species and coupled with an alkaline $Zn(OH)_4^{2-}$/Zn anode to compose a hybrid electrolyte all-aqueous RFB. Eqn (3) illustrates the redox action of I_3^-/I^- *via* two-electron transfer. Iodide has been recognized as one of the most promising cathode redox candidates owing to the following reasons. Firstly, benefiting from its high solubility (over 8 mol L^{-1}) in aqueous electrolyte, iodide has the ability to deliver high energy density.[25] Moreover, the suitable I_3^-/I^- redox potential (0.536 V *vs.* SHE) makes it possible to avoid water electrolysis.[35]

$$I_3^- + 2e^- \rightarrow 3I^- \quad E^0 = 0.536\ \text{V} \tag{3}$$

$$I_2(s) + I^- \leftrightarrow I_3^- \quad K = 723 \pm 10\ (25\ ^\circ\text{C}) \tag{4}$$

As in eqn (4), I_3^- can be constructed by the addition of solid I_2 into an I^- solution (potassium iodide (KI) solution was employed in this work).[26,30] The solubility of I_2 will dramatically improve with the presence of excess I^-. With the increasing concentration of I_2, other polyiodide species (such as I_5^-, I_7^-, and I_9^-) will also be formed. But, I_3^- is the predominant electroactive species and the only isolated polyiodide that exists in aqueous solution.[36] During discharge (Fig. 1a), zinc oxidation reaction occurs at the anode in an alkaline potassium hydroxide (KOH) anolyte, yielding soluble zincate ($Zn(OH)_4^{2-}$) ions and liberated electrons. The electrons travel through an external circuit from the anode to the cathode, producing electricity. I_3^- is reduced into I^- at the cathode once having received the electrons. At the same time, K^+ migrates from the anode to the cathode to complete the reaction. During charge (Fig. 1b), the reverse redox reactions occur at the two electrodes, in which zincate is reduced into zinc deposited onto the anode, while I^- is oxidized back to I_3^- at the cathode. Meanwhile, K^+ travels through the membrane from the cathode to the anode. The overall working principle of the proposed alkaline anolyte Zn–I_2 RFB can be described as follows:

$$\text{Anode: } Zn(OH)_4^{2-} + 2e^- \rightarrow Zn + 4OH^- \quad E^0 = -1.260\ \text{V} \tag{5}$$

$$\text{Cathode: } I_3^- + 2e^- \rightarrow 3I^- \quad E^0 = 0.536\ \text{V} \tag{6}$$

$$\text{Overall: } Zn + I_3^- + 4OH^- \leftrightarrow Zn(OH)_4^{2-} + 3I^- \quad E^0 = 1.796\ \text{V} \tag{7}$$

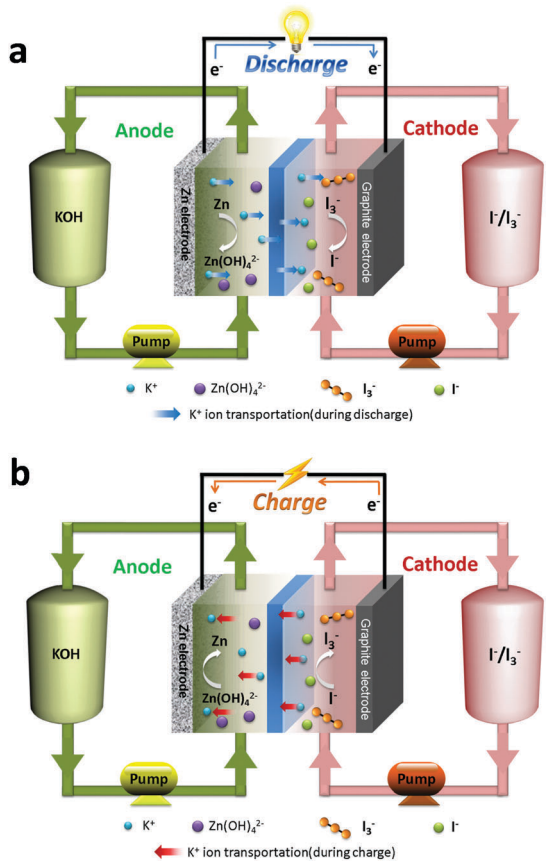

Fig. 1 Schematic illustration of the working principle of (a) discharge and (b) charge processes of the designed alkaline Zn–I_2 redox flow battery.

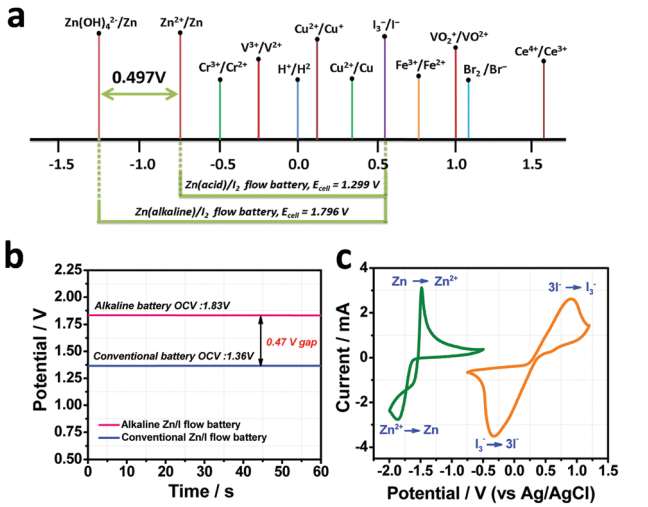

Fig. 2 (a) The standard redox potentials of various candidate redox pairs suitable for the all-aqueous redox flow battery. (b) The open-circuit-voltage between the conventional and designed alkaline Zn–I_2 redox flow battery. (c) Cyclic voltammograms of 0.1 M $ZnAc_2$ with 3 M KOH (green curve) and 0.1 M KI (yellow curve) on a glassy carbon electrode at a scanning rate of 50 mV s^{-1}.

Theoretically, this newly-designed alkaline Zn–I_2 RFB outweighs its conventional counterparts by a 0.497 V (Fig. 2a) increase in battery voltage and a 38.26% enhancement in energy density (see the calculation details in the ESI†), which is a very significant improvement. The practical demonstration of open circuit voltage (Fig. 2b) also shows a real 0.47 V potential gap existing between the two batteries. In particular, as shown in Fig. 2c, cyclic voltammetry (CV) measurements of 0.1 M zinc acetate ($ZnAc_2$) with a 3 M KOH solution were performed to determine the potentials of the $Zn(OH)_4^{2-}$/Zn redox pair. A typical voltammogram shape of zinc electrodeposition is illustrated without a hydrogen evolution peak. Also, a cyclic voltammogram of 0.1 M KI electrolyte shows the pair of the I_3^-/I^- redox reaction with no oxygen evolution reaction being observed throughout the entire scan range. All of these features demonstrate the feasibility and superiority of the alkaline Zn–I_2 RFB.

The evaluation of the battery performance was conducted at different current densities (10–100 mA cm^{-2}). In order to keep the osmolarity balanced, equivalent concentrations of KOH anolyte solution and KI/I_2 catholyte solution were prepared in each external electrolyte reservoir. A polymer membrane (Nafion 117) was assembled between the two electrodes to limit the migration of negative ions. As shown in Fig. 3a, the battery specific capacity was investigated at a constant current density of 20 mA cm^{-2} as a function of the concentration of KI/I_2 catholyte solution. High practical specific capacities were successfully obtained from 80.0 (2 M) to 193.5 A h L^{-1} catholyte (6 M) with the increase in catholyte concentration. But, these impressive specific capacities are still considerably lower than the theoretical values (Fig. 3b). The loss of capacity comes from the result of three things. (1) Polyiodide formation: as discussed above, the I_3^- solution can be obtained by the dissolution of I_2 into KI solution.

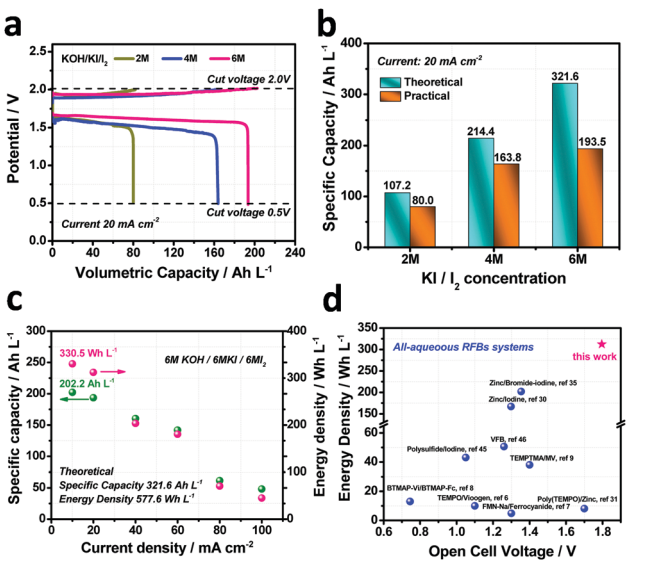

Fig. 3 (a) Representative galvanostatic charge and discharge curves at different electrolyte concentrations at a current density of 20 mA cm^{-2}. (b) The practical specific capacity compared with the theoretical values as a function of the catholyte concentration. (c) Influence of the discharging current density on the achievable specific capacity and energy density. (d) Diagram of the energy density of all-aqueous redox flow batteries prepared in recent years compared with the value in this work.

Ideally, an equal amount of I_2 reacts with KI solution, aiming at obtaining an equal amount of I_3^- solution according to eqn (4). However, in addition to I_3^- ions, some extended polyiodide compounds can also be formed through interactions between fundamental blocks: I_2, I^-, and I_3^-.[36] Therefore, the practical amount of I_3^- ions cannot reach the theoretical value as desired, leading to the loss of capacity compared to the theoretical values. (2) Electrolyte crossover: the cationic exchange Nafion membrane was assembled between the anode and the cathode to resist the movement of any existing $Zn(OH)_4^{2-}$, I_3^-, and I^- anions, whereas K^+ ions as a mediator can smoothly shuttle between the two electrodes to conduct the charges in the battery. Energy-dispersive X-ray spectroscopy (EDX) was used to investigate the Nafion membrane after discharge on both the anode and cathode sides to confirm the elements existing in the membrane (Table S1, ESI†). The EDX result reveals that the Zn and I elements are present on both sides of the membrane, indicating that the electrolyte crossover issue exists in this system. The reason can be ascribed to the hydrophilic nature of the membrane. Nafion membrane is a hydrophilic polymer which conducts ions with the assistance of water molecules. Inevitably, a small number of hydrated anions will still pass through the membrane along with water molecules. In order to investigate the electrolyte crossover issue, the permeability of the zincate ($Zn(OH)_4^{2-}$) ion was investigated (Fig. S7, ESI†). Two different concentrations of KOH solution (2 M and 6 M) were prepared in the left compartment with the corresponding concentrations of KI solution in the right compartment to simulate the actual battery conditions. Saturated zincate ($Zn(OH)_4^{2-}$) ion solutions were prepared in the left compartment to create maximum ion crossover environments. As shown in Fig. S7 (ESI†), the concentration of zincate ($Zn(OH)_4^{2-}$) ions in the right compartment increases with the increase of permeation time in both 2 M and 6 M KI solutions. The permeability coefficients of zincate ($Zn(OH)_4^{2-}$) ions across Nafion 117 obtained are 6.74×10^{-7} cm^2 min^{-1} and 11.62×10^{-7} cm^2 min^{-1} in 2 M and 6 M prepared electrolytes, respectively. Overall, K^+ ions exist in both reservoirs and can smoothly shuttle between the two electrodes to conduct the charges in the battery. Hydroxide (OH^-) ions in the left reservoirs continuously react with zinc to form a solution of potassium zincate ($Zn(OH)_4^{2-}$). For a vanadium redox flow battery (VRFB) system, low vanadium permeability is essential for the membrane. Compared with the latest reported VRFB with ultra-low vanadium permeability, the Nafion 117 membrane in our system still exhibits comparable performance with low ion permeability. Overall, the vast majority of anions have been blocked by the Nafion membrane and have reacted in their individual electrolyte reservoir, but still a small amount of undesired hydrated $Zn(OH)_4^{2-}$, I_3^-, and I^- ions was able to go across the membrane, which finally results in the loss of some battery capacity. (3) Polarization: In this work, graphite foil was used as a current collector for the I_3^-/I^- redox reaction to simply demonstrate the design for this alkaline Zn–I_2 RFB. However, the graphite foil largely limited the battery performance because of its low surface area. Even though it is in the preliminary design stage, the alkaline Zn–I_2 RFB still exhibited distinguished performance. As shown in Fig. 3c, the alkaline Zn–I_2 RFB can run in a wide current density region from 10 to 100 mA cm^{-2}. With the decrease of the employed current density, the battery produced more electricity and finally reached a remarkable specific capacity of 202.2 A h $L^{-1}_{catholyte}$. Benefiting from the high voltage design of this alkaline Zn–I_2 RFB, a prominent energy density of 330.5 W h $L^{-1}_{catholyte}$ was achieved at 10 mA cm^{-2}, which is the highest energy density obtained to date in an all-aqueous RFB system to the best of our knowledge. The diagram in Fig. 3d shows a summary of the performance of various all-aqueous RFBs. With respect to battery potential and energy density, the alkaline Zn–I_2 RFB shows the best performance among all conventional or newly-emerged redox flow batteries.

To investigate the battery's ability to maintain its high energy density, the cycling performance of the alkaline Zn–I_2 RFB was investigated through long-term 20 hour per cycle testing at a current density of 20 mA cm^{-2}, which is a 44% depth of discharge cycles according to the theoretical battery capacity. As shown in Fig. 4a and b, the battery achieved a 100% coulombic efficiency during all 10 cycles (200 h), but the voltage and energy efficiencies exhibited fluctuations from 65% to 80%. The main reasons come from three processes on the zinc plate anode: passivation, electrode shape change and zinc dendrite formation.[34] During discharge, zinc is generally dissolved into the alkaline electrolyte, producing $Zn(OH)_4^{2-}$ ions in the anolyte. However, if there is not enough OH^- offered in the anolyte and the $Zn(OH)_4^{2-}$ ions reach their solubility limit, an insulating ZnO film will be produced and precipitated on the electrode surface, causing an increase in the internal resistance of the electrode.[37] Also, during charge, zinc will be deposited back onto the electrode but at a different position, resulting in the shape change of the zinc electrode and a loss of usable capacity. Furthermore, zinc dendrites are also observed during charge due to the result of concentration-controlled zinc electrodeposition.[33,38,39] Therefore, after each three or four cycles, a fresh zinc plate was used to replace the exhausted zinc electrode to achieve stable energy density. Finally, an energy density of $\sim$200 W h L^{-1} was obtained during all of the cycles (200 h), which is the highest reported cycling energy density for an all-aqueous RFB. The cycling performance of the alkaline Zn–I_2 RFB was also investigated through short-term cycles with long-term stability. In the short-term cycling testing, the discharge and charge cycling performance of the battery was evaluated using a pulse cycling technique with each short 2 hour cycle at a current density of 10 mA cm^{-2}. As shown in Fig. 4c, the battery has a fluctuating charge voltage within the first 40 hours. This is because during the very early stages, short term discharge cannot produce enough $Zn(OH)_4^{2-}$ (in anolyte) and I^- (in catholyte) to afford a charge of the same time length, thus leading to an unstable performance in charge processing in the first 40 hours. Afterwards, the battery exhibits a very small polarization with a charge–discharge voltage gap of 0.35 V. Even at 140 hours, the discharge voltage was still above 1.5 V with a corresponding charge voltage at around 2.0 V. During the overall 70 cycles (140 h), the battery displayed an excellent coulombic efficiency of 100% and a promising voltage/energy efficiency of 80% (in Fig. 4d), which demonstrates the superior cycling stability of this alkaline Zn–I_2 RFB.

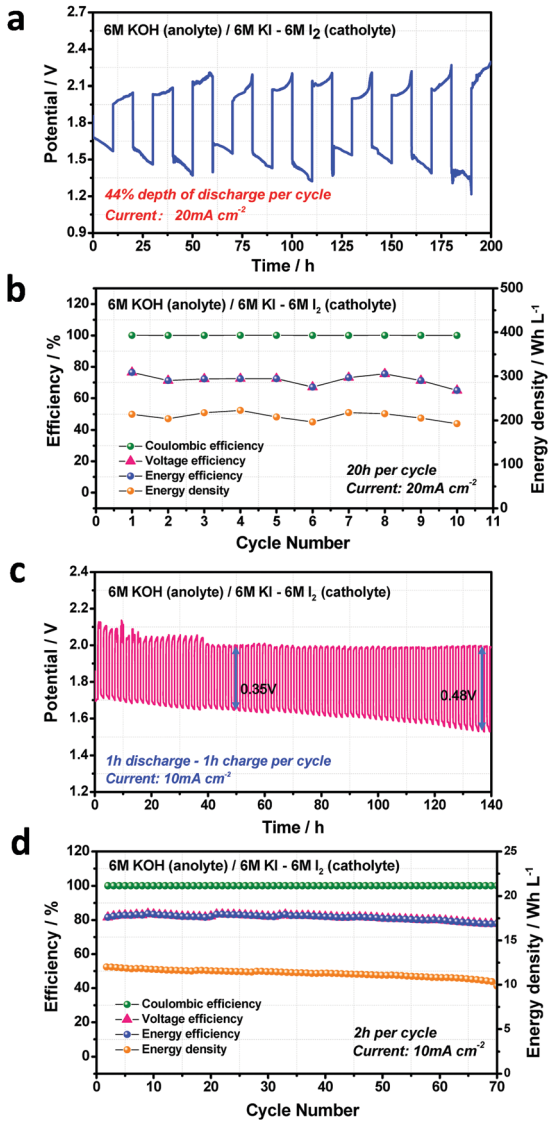

Fig. 4 (a) Long-term cell cycling performance of the voltage curve at 20 mA cm^{-2} and (b) the corresponding coulombic efficiency (CE), voltage efficiency (VE), energy efficiency (EE), and energy density of the experimental Zn–I_2 RFB. (c) Short-term cell cycling performance of the voltage curve at 10 mA cm^{-2} and (d) the corresponding CE, VE, EE, and energy density of the experimental Zn–I_2 RFB.

Conclusions

In summary, a novel strategy towards a high energy density all-aqueous redox flow battery has been put forward in this work. Theoretically, high energy density can be achieved by enhancing the battery voltage, and the electrolyte acidic/basic properties have a great influence on the redox pair potential. Thus, by tuning the pH of the electrolyte, the battery voltage can be effectively enhanced, finally leading to an increase in energy density. With this strategy, we demonstrate an all-aqueous alkaline Zn–I_2 RFB achieving a high-energy-density of 330.5 W h L^{-1} with a 0.47 V anode potential enhancement compared to the conventional counterparts, which is the highest energy density for an all-aqueous redox flow battery obtained to date. In addition, the alkaline Zn–I_2 RFB also exhibits a promising cycling performance with 100% coulombic efficiency, ~70% voltage and energy efficiency and a high energy density of ~200 W h L^{-1} maintained over 200 h. However, though these preliminary results are promising, numerous challenges still exist such as the electrolyte preparation issue, electrolyte crossover problem, electrode polarization, *etc.* More studies are needed to perfect this system in the future, for example the development of a separator membrane, highly active electrocatalyst and advanced cell design.[40–46] Overall, this alkaline Zn–I_2 RFB system demonstrates a new design with promising performance for an all-aqueous redox flow battery, and more importantly, opens a feasible and effective approach for achieving high-voltage high-energy-density all-aqueous electrochemical energy devices.

Conflicts of interest

There are no conflicts to declare.

Acknowledgements

J. Z. and G. J. contributed equally to this work. The present study was financially supported by the Natural Sciences and Engineering Research Council of Canada (NSERC) through grants to Z. C. and the University of Waterloo.

References

1 W. Wang and V. Sprenkle, *Nat. Chem.*, 2016, **8**, 204–206.
2 J. Winsberg, T. Hagemann, T. Janoschka, M. D. Hager and U. S. Schubert, *Angew. Chem., Int. Ed.*, 2017, **56**, 686–711.
3 W. Wang, Q. Luo, B. Li, X. Wei, L. Li and Z. Yang, *Adv. Funct. Mater.*, 2013, **23**, 970–986.
4 Z. P. Cano, D. BBanham, S. Ye, A. Hintennach, J. Lu, M. Fowler and Z. Chen, *Nat. Commun.*, 2018, 279–289.
5 B. Huskinson, M. P. Marshak, C. Suh, S. Er, M. R. Gerhardt, C. J. Galvin, X. Chen, A. Aspuru-Guzik, R. G. Gordon and M. J. Aziz, *Nature*, 2014, **505**, 195–198.
6 T. Janoschka, N. Martin, U. Martin, C. Friebe, S. Morgenstern, H. Hiller, M. D. Hager and U. S. Schubert, *Nature*, 2015, **527**, 78–81.
7 A. Orita, M. G. Verde, M. Sakai and Y. S. Meng, *Nat. Commun.*, 2016, **7**, 13230.
8 E. S. Beh, D. De Porcellinis, R. L. Gracia, K. T. Xia, R. G. Gordon and M. J. Aziz, *ACS Energy Lett.*, 2017, **2**, 639–644.
9 T. Janoschka, N. Martin, M. D. Hager and U. S. Schubert, *Angew. Chem., Int. Ed.*, 2016, **55**, 14427–14430.
10 K. Lin, R. Gómez-Bombarelli, E. S. Beh, L. Tong, Q. Chen, A. Valle, A. Aspuru-Guzik, M. J. Aziz and R. G. Gordon, *Nat. Energy*, 2016, **1**, 16102.
11 C. S. Sevov, D. P. Hickey, M. E. Cook, S. G. Robinson, S. Barnett, S. D. Minteer, M. S. Sigman and M. S. Sanford, *J. Am. Chem. Soc.*, 2017, **139**, 2924–2927.
12 W. Wang, W. Xu, L. Cosimbescu, D. Choi, L. Li and Z. Yang, *Chem. Commun.*, 2012, **48**, 6669–6671.

13 T. Liu, X. Wei, Z. Nie, V. Sprenkle and W. Wang, *Adv. Energy Mater.*, 2016, **6**, 1501449.
14 X.-P. Gao and H.-X. Yang, *Energy Environ. Sci.*, 2010, **3**, 174–189.
15 L. Chen, Z. Guo, Y. Xia and Y. Wang, *Chem. Commun.*, 2013, **49**, 2204–2206.
16 F. R. Brushett, J. T. Vaughey and A. N. Jansen, *Adv. Energy Mater.*, 2012, **2**, 1390–1396.
17 H. Chen, Q. Zou, Z. Liang, H. Liu, Q. Li and Y. C. Lu, *Nat. Commun.*, 2015, **6**, 5877.
18 Y. Ding, Y. Zhao, Y. Li, J. B. Goodenough and G. Yu, *Energy Environ. Sci.*, 2017, **10**, 491–497.
19 W. Duan, J. Huang, J. A. Kowalski, I. A. Shkrob, M. Vijayakumar, E. Walter, B. Pan, Z. Yang, J. D. Milshtein, B. Li, C. Liao, Z. Zhang, W. Wang, J. Liu, J. S. Moore, F. R. Brushett, L. Zhang and X. Wei, *ACS Energy Lett.*, 2017, **2**, 1156–1161.
20 Q. Huang, J. Yang, C. B. Ng, C. Jia and Q. Wang, *Energy Environ. Sci.*, 2016, **9**, 917–921.
21 X. Wei, W. Xu, M. Vijayakumar, L. Cosimbescu, T. Liu, V. Sprenkle and W. Wang, *Adv. Mater.*, 2014, **26**, 7649–7653.
22 Y. Yang, G. Zheng and Y. Cui, *Energy Environ. Sci.*, 2013, **6**, 1552.
23 X. Wei, L. Cosimbescu, W. Xu, J. Z. Hu, M. Vijayakumar, J. Feng, M. Y. Hu, X. Deng, J. Xiao, J. Liu, V. Sprenkle and W. Wang, *Adv. Energy Mater.*, 2015, **5**, 1400678.
24 N. Li, Z. Weng, Y. Wang, F. Li, H.-M. Cheng and H. Zhou, *Energy Environ. Sci.*, 2014, **7**, 3307–3312.
25 Y. Zhao, M. Hong, N. Bonnet Mercier, G. Yu, H. C. Choi and H. R. Byon, *Nano Lett.*, 2014, **14**, 1085–1092.
26 Y. Zhao, L. Wang and H. R. Byon, *Nat. Commun.*, 2013, **4**, 1896.
27 Y. Ding and G. Yu, *Angew. Chem., Int. Ed.*, 2016, **55**, 4772–4776.
28 R. M. Darling, K. G. Gallagher, J. A. Kowalski, S. Ha and F. R. Brushett, *Energy Environ. Sci.*, 2014, **7**, 3459–3477.
29 S. Gu, K. Gong, E. Z. Yan and Y. Yan, *Energy Environ. Sci.*, 2014, **7**, 2986–2998.
30 B. Li, Z. Nie, M. Vijayakumar, G. Li, J. Liu, V. Sprenkle and W. Wang, *Nat. Commun.*, 2015, **6**, 6303.
31 J. Winsberg, T. Janoschka, S. Morgenstern, T. Hagemann, S. Muench, G. Hauffman, J. F. Gohy, M. D. Hager and U. S. Schubert, *Adv. Mater.*, 2016, **28**, 2238–2243.
32 B. Beverskog and I. Puigdomenech, *Corros. Sci.*, 1997, **39**, 107–114.
33 P. Delahay, M. Pourbaix and P. V. Rysselberghe, *J. Electrochem. Soc.*, 1951, **98**, 101–105.
34 J. Fu, Z. P. Cano, M. G. Park, A. Yu, M. Fowler and Z. Chen, *Adv. Mater.*, 2017, 29.
35 G.-M. Weng, Z. Li, G. Cong, Y. Zhou and Y.-C. Lu, *Energy Environ. Sci.*, 2017, **10**, 735–741.
36 P. H. Svensson and L. Kloo, *Chem. Rev.*, 2003, **103**, 1649–1684.
37 Y. Li and H. Dai, *Chem. Soc. Rev.*, 2014, **43**, 5257–5275.
38 J. Zhang, J. Fu, X. Song, G. Jiang, H. Zarrin, P. Xu, K. Li, A. Yu and Z. Chen, *Adv. Energy Mater.*, 2016, **6**, 1600476.
39 J. Fu, F. M. Hassan, C. Zhong, J. Lu, H. Liu, A. Yu and Z. Chen, *Adv. Mater.*, 2017, **29**, 1702526.
40 W. A. Braff, M. Z. Bazant and C. R. Buie, *Nat. Commun.*, 2013, **4**, 2346.
41 Z. Yuan, Y. Duan, H. Zhang, X. Li, H. Zhang and I. Vankelecom, *Energy Environ. Sci.*, 2016, **9**, 441–447.
42 Z. Yuan, X. Zhu, M. Li, W. Lu, X. Li and H. Zhang, *Angew. Chem., Int. Ed.*, 2016, **55**, 3058–3062.
43 Y. Zhao, M. Li, Z. Yuan, X. Li, H. Zhang and I. F. J. Vankelecom, *Adv. Funct. Mater.*, 2016, **26**, 210–218.
44 B. Li, J. Liu, Z. Nie, W. Wang, D. Reed, J. Liu, P. McGrail and V. Sprenkle, *Nano Lett.*, 2016, **16**, 4335–4340.
45 Z. Li, G. Weng, Q. Zou, G. Cong and Y.-C. Lu, *Nano Energy*, 2016, **30**, 283–292.
46 S. Roe, C. Menictas and M. Skyllas-Kazacos, *J. Electrochem. Soc.*, 2015, **163**, A5023–A5028.